Experimental and Numerical Study of the Effect of Openings on the Surface Pressure Distribution of a Hollow Cube

M. PETRIDOU and D. BOURIS
Department of Engineering and Management of Energy Resources
University of Western Macedonia
Bakola & Sialvera, 50100, Kozani
GREECE

Abstract: Infiltration and natural ventilation for a simplified cubic building structure is considered through an experimental and numerical study of building envelope surface pressure distribution, as affected by openings on its vertical sides. The envelope outer surface pressure distribution is experimentally studied in a wind tunnel, using a plexiglass hollow cube model and varying the relative positions of the openings. The measurements are subsequently used for validation of a computational fluid dynamics methodology. Turbulence was modelled using a modification to the standard k-ε model for improved accuracy in flows past bluff bodies. Results indicate significant influence of the relative positions of the openings in the variation of the pressure distribution, as compared to the case of a solid cube. Sabstantial improvement in the predictions is observed when using the modification to the k-ε turbulence model, especially in areas of flow separation following stagnation regions.

Key-Words: - CFD, Cube, Pressure distribution, Turbulence modeling, Ventilation

1 Introduction

Infiltration and natural ventilation rates are significantly affected by incident wind flow on the outer surfaces of a building. The envelope outer surface pressure distribution interacts with the building's inner pressure and determines one of the principle infiltration and ventilation driving forces, the other being the stack effect due to temperature/density variations. Convective heat transfer is also influenced by the outer flow past the building and strongly influences heating and cooling loads. The above mentioned effects are both three dimensional and transient in nature, rendering numerical studies of the dominant phenomena a challenging task.

Infiltration and ventilation can be simulated using a variety of numerical models from the literature but most use simplified nodal approaches and assume fixed outer pressure distribution rather than calculating it [1]. More recent studies attempt to include three dimensional approaches implementing computational fluid dynamics (CFD) although usually only the outer building environment is considered and the effect of the flow through openings in the envelope is most often ignored [2]. Looking at the problem in more depth, the numerical modeling of flow past bluff bodies, even without openings, is by no means a trivial task. Efforts include specific modifications to standard turbulence models [3] as well as large eddy simulations [4].

The present work is part of an ongoing effort to include fully three dimensional effects in the simulation of flow and heat transfer through a building envelope. Here, computational fluid dynamics (CFD) is used to isothermally calculate the air flow past the envelope and through the openings of a simplified building structure. Experimental measurements have also been performed in a wind tunnel under highly confined conditions in order to provide validation data for calculation of the pressure distribution on the outer surfaces. A study is performed of the effect of placing openings at various positions on the vertical sides of the structure and turbulence modelling issues are addressed through an easily implemented modification that has been proposed in the literature [3].

2 Experimental Measurements

Experimental measurements have been performed for the outer surface pressure distribution on a solid cube and on cubes with various openings on their side walls. A simplified cubic building (height:

H=20 cm) made of plexiglass (thickness=0.04H) was placed in a wind tunnel of 35 cm square cross section with an oncoming flow corresponding to a Reynolds number of Re_H=165112. A total of eight openings were then cut out of the four vertical sides of the cube (Fig. 1) and measurements were repeated at the same flow conditions but with different combinations of the openings left open: a) 2 openings on all four sides, b) 2 openings on upstream face, c) 2 openings on upstream and downstream face, d) 2 openings on downstream face. The highly confined conditions may not be representative of a free standing structure but they can be considered relevant to what would arise in the close proximity of neighbouring structures and they also provide a very well defined domain for validation of numerical studies.

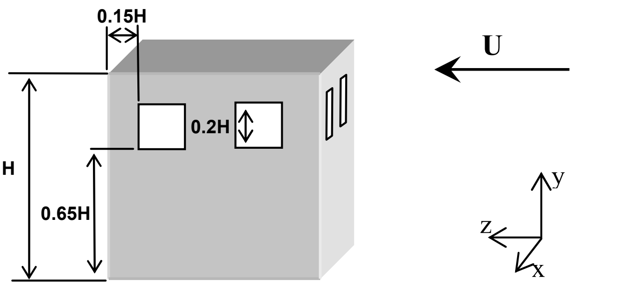

Fig. 1. Geometry of cube with openings used in the experimental measurements.

A pitot-static tube connected to an electronic manometer was used to measure upstream velocity profiles at 10 spanwise positions, 1.5H upstream of the cube center. The measured velocity distributions are presented in Fig. 2.

For the measurement of the surface pressure distribution, there were a total of 32 pressure taps (1.2mm diameter) drilled into the cube: 23 on one of the side faces and 9 on the top. Each pressure tap lead to an independent silicon tube which was in turn connected to a system of corresponding plastic valves that could be manipulated to allow pressure measurement with any selected pressure tap, through the manometer. The tubing ran flush with the inner walls of the cube so as to avoid, as much as possible, any interference with the flow passing through the openings. By rotating the cube, the pressure distribution on the top and four sides were acquired. Ten pressure measurements were made for each point at 1 sec intervals and the mean value was used to determine the static pressure difference (Δp) between each point and the static pressure of the flow 1.5H upstream of the cube center at the cube height. The reference pressure does not correspond to the free stream due to the confinement of the flow, but it does correspond to the same position as the velocity profile measurements, allowing validation of the numerical studies as long as the inlet of the computational domain coincides with the measured reference position. The measured pressure differences are presented in non-dimensional form ($\Delta p/0.5\rho U^2$) along with the numerical calculations in a following section. Measurement statistical uncertainty was found to be below 10% with the exception of a couple of points in stagnation regions where it reached a maximum of 18%.

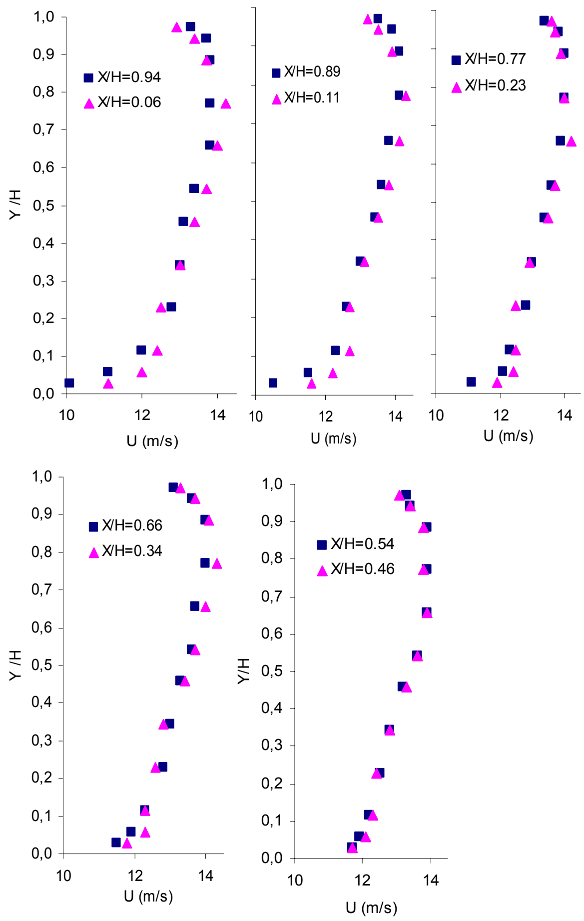

Fig. 2. Velocity profiles 1.5H upstream of the cube centre and at ten spanwise positions of the wind tunnel.

3 Numerical Methodology

The Reynolds averaged Navier Stokes (RANS) and temperature equations are solved by volume averaging on a collocated Cartesian grid using the SIMPLE algorithm [5], [6]. The general form of the momentum (in the three coordinate directions), mass, turbulent kinetic energy and turbulent energy dissipation equations is:

$$\frac{\partial(\rho u \Phi)}{\partial x}+\frac{\partial(\rho v \Phi)}{\partial y}+\frac{\partial(\rho w \Phi)}{\partial z}= \frac{\partial}{\partial x}(\Gamma_\Phi \frac{\partial \Phi}{\partial x})+\frac{\partial}{\partial y}(\Gamma_\Phi \frac{\partial \Phi}{\partial y})+\frac{\partial}{\partial z}(\Gamma_\Phi \frac{\partial \Phi}{\partial z})+S_\Phi \quad (1)$$

where (Φ)=(u), (v), (w), (1), (k), (ε) respectively and (S_Φ) represents the source terms including pressure terms etc., as appropriate for the variable (Φ) being solved ([5]). The diffusion coefficients (Γ_Φ) are:

$$\Gamma_\Phi=\frac{\mu}{Pr}+\frac{\mu_t}{\sigma_T}, \qquad \mu_{eff}=\mu+\mu_t \quad (2)$$

where (μ_{eff}) is the effective turbulent viscosity, (μ) is the fluid viscosity, (μ_t) is the turbulent eddy viscosity and σ_T=1. For upwind differencing of the convective terms, the fully bounded second order BSOU scheme was used [7].

Turbulence is modeled using the MMK modification to the standard k-ε model since it has proven to alleviate deficiencies related to overestimation of turbulence kinetic energy production (P_k) in stagnation regions such as those that form on the upwind side of bluff bodies [3]. More specifically, the source term for turbulent kinetic energy (k) in (1) is expressed as:

$$S_k=P_k-\rho\varepsilon=P_k-C_\mu\rho^2k^2/\mu_t \quad (3)$$

where C_μ=0.09 is a model constant and the production of turbulent kinetic energy (P_k) when implementing the standard k-ε model is:

$$P_k=\nu_t S^2,\ \nu_t=C_\mu\frac{k^2}{\varepsilon},\ S=\sqrt{\frac{1}{2}\left(\frac{\partial<u_i>}{\partial x_j}+\frac{\partial<u_j>}{\partial x_i}\right)^2} \quad (4)$$

The MMK modification ([3]) requires that when $\Omega/S<1$, C_μ is replaced by C_μ^*:

$$C_\mu^*=C_\mu\frac{\Omega}{S}, \qquad \Omega=\sqrt{\frac{1}{2}\left(\frac{\partial<u_i>}{\partial x_j}-\frac{\partial<u_j>}{\partial x_i}\right)^2} \quad (5)$$

where (Ω) and (S) are the vorticity scale and the strain rate respectively.

4 Computational Details and Results

4.1 Validation for solid cube

The numerical methodology was first implemented for the solid cube case studied experimentally in order to evaluate the ability of the model to calculate pressure distributions on the outer surfaces of the cube. A 64x51x91 numerical grid (Grid 1) was constructed to fit the wind tunnel cross section (1.75Hx1.75H) and a total of 7.5H in the flow direction. There were 30 grid points on the cube edge and the cube was positioned 1.5H from the inlet so that the measured velocity profile (Fig. 2) could be used as an inlet boundary condition. Both the standard k-ε model and the MMK modification were used and then the MMK modification was implemented using a denser grid: 75x62x102 with 40 grid points on the cube edge (Grid 2). The computational domain and inlet velocity profile were kept the same.

4.2 Validation for cube with openings

The numerical methodology was subsequently implemented for the cases with openings in the cube envelope. For the case with openings on all four sides, the same grids used for the solid cube were implemented. There were 30 (Grid 1) or 40 (Grid 2) grid points on the cube edge and the cube was positioned 1.5H from the inlet. Again, the measured velocity profile of Fig. 2 was used as an inlet boundary condition. For the remaining three cases (openings on the upstream face, the upstream and downstream faces, and the downstream face), only the denser grid was used (Grid 2) with all other geometrical parameters and boundary conditions kept constant.

4.3 Results

Streamlines of the flow field, as calculated by the numerical methodology, are presented in Fig. 3 through Fig. 7. The recirculation zones forming on the top and side can be seen in Fig. 3 along with the stagnation region and horseshoe vortex that begins to form near the ground on the upstream side. However, as discerned in Fig. 4 as well, the vortex is forced to compress along the cube sides due to the confinement of the flow.

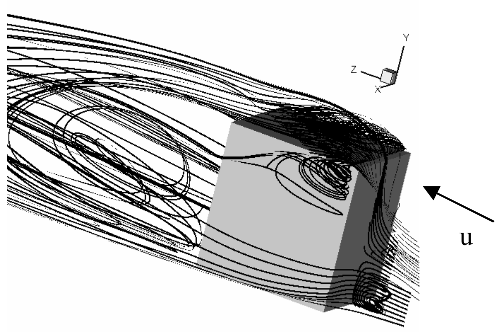

Fig. 3. Flow field past the solid cube.

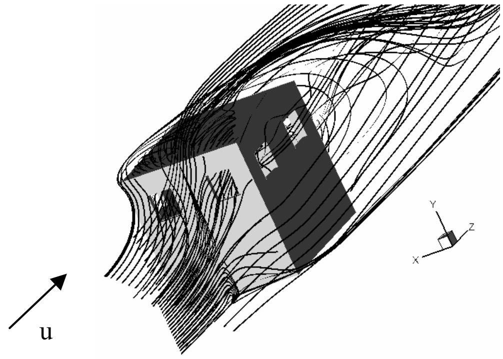

Fig. 4. Flow field past the cube with openings on all four sides.

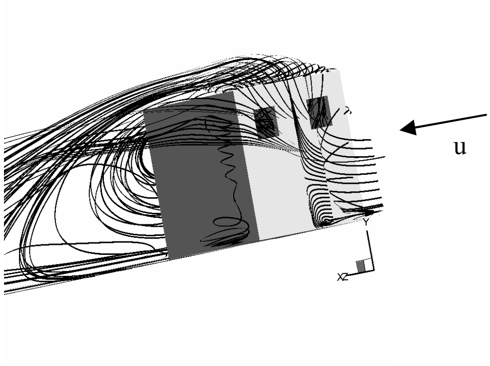

Fig. 5. Flow field past the cube with openings on the upwind face.

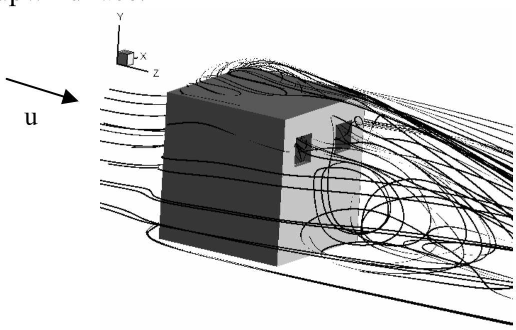

Fig. 6. Flow field past the cube with openings on both the upwind and downstream faces.

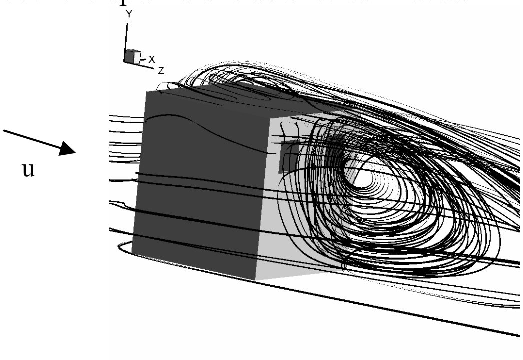

Fig. 7. Flow field past the cube with openings on the downstream face.

Generally, there are important changes in the flow structure due to the presence of the openings, and some local differences can be commented upon. The recirculation zones forming on the side can be seen in Fig. 3 and Fig. 5 and it is into these that the side openings of Fig. 4 release the flow from inside the cube. However, even the flow that enters from the upstream openings and manages to exit from the sides is forced to closely follow the side face and most definitely disrupts the structure of the side face recirculation zones. In Fig. 4, a second stagnation region is also discernable above the openings and below the top leading edge. For the solid cube case (Fig. 3) the same region is influenced by the flow leaving the stagnation region and heading towards separation from the top leading edge. The downstream recirculation zone behind the cube is the largest (discernable in Fig. 3-Fig. 7) and it is interesting to note how the openings on the downstream face interact with this (Fig. 6, Fig. 7). When there is flow entering through the upstream openings, this exits downstream, enters the rear recirculation zone and is carried downstream. If only the downstream openings are present, there is an insignificant amount of flow entering (or leaving) the cube and the recirculating flow behind the cube will only slightly interact with the indoor air.

Comparison of the measured and calculated pressure distribution on the sides of the solid cube and the cube with openings is shown in Fig. 8 through Fig. 11. On the top of the cube, the openings allow for flow through the building and reduce the suction pressure that appears in the recirculation zone. This is especially evident at about 0.25H from the leading edge (Fig. 8) where the solid cube shows a minimum pressure coefficient of -4 and the other cases with openings barely reach a value of -3.5.

At the upstream face (Fig. 9), the pressure distribution remains much the same near the floor (Y/H=0.25) but leads to an interesting behaviour at the level of the openings (Fig. 9b-e). When there is cross flow through the cube, i.e. when upstream and downstream openings are simultaneously present, the pressure values drop near the upstream openings (Fig. 9 b,d) indicating high flow velocities entering the cube. When there is no cross path through the cube, the pressure levels remain almost the same on the upstream face, regardless of the presence of upstream openings (Fig. 9c,e). It is interesting to note that when the side openings are present (Fig. 9b) the pressure levels are lower than when they are not. As will be shown later, the side openings enhance the flow entering the building.

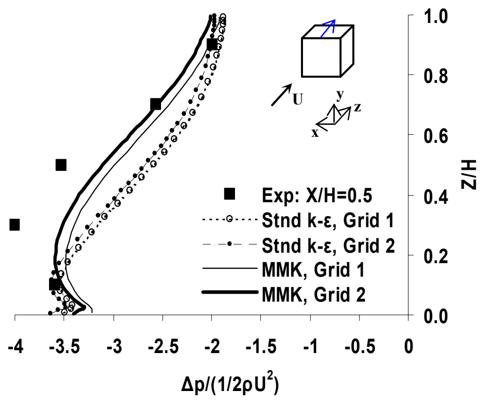

a)

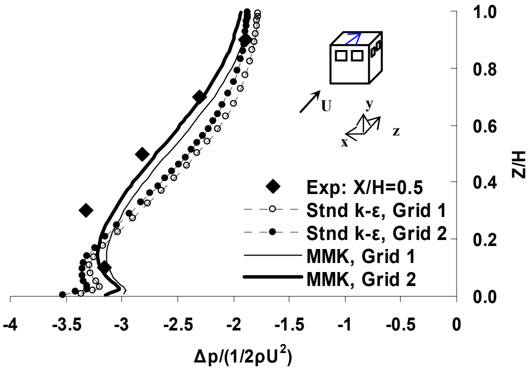

b)

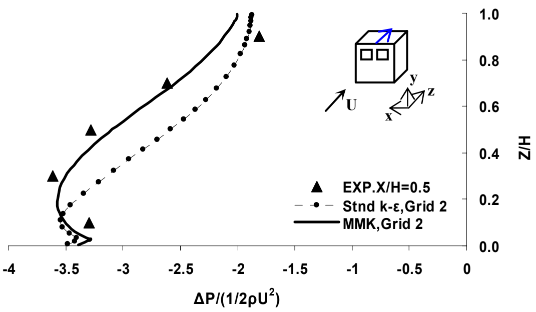

c)

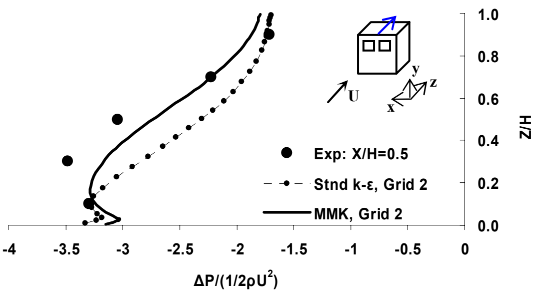

d)

Fig. 8. Pressure distribution in the flow direction (z) on the top of the a) solid cube, b) cube with openings on all faces (Fig. 1), c) cube with openings on the upwind face, and d) cube with openings on the upwind and downstream faces.

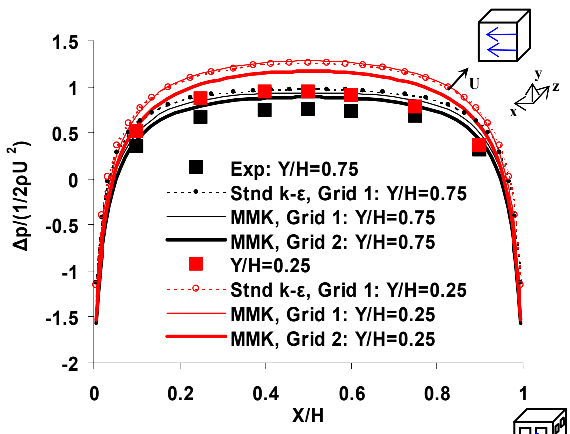

a)

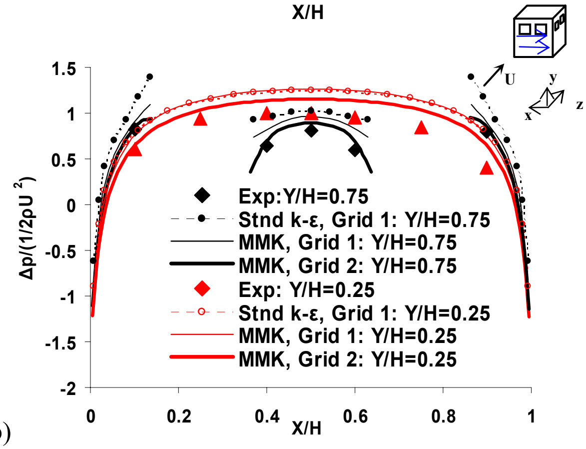

b)

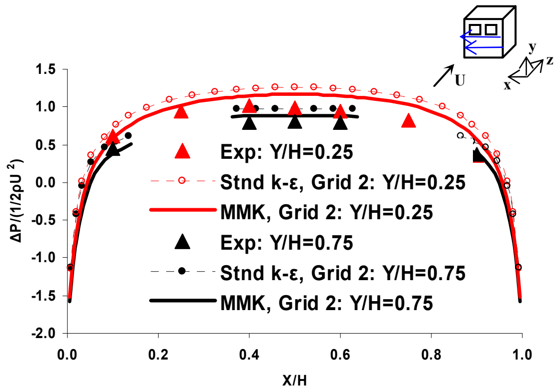

c)

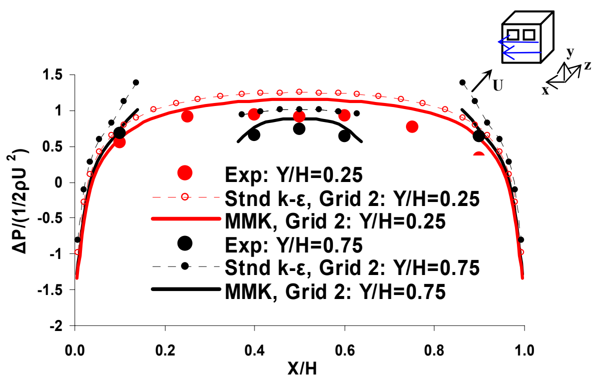

d)

Fig.9. Figure caption on next page

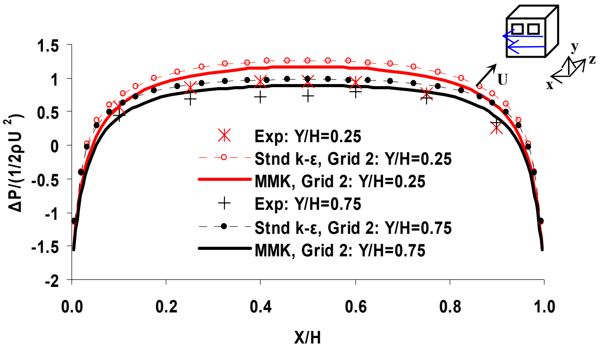

e)

Fig. 9. (continued) Pressure distribution on the upwind face at 0.25 and 0.75 of the cube height for a) solid cube, b) cube with openings on all faces (Fig. 1), c) cube with openings on the upwind face, d) cube with openings on the upwind and downstream faces, and e) cube with openings on the downstream face.

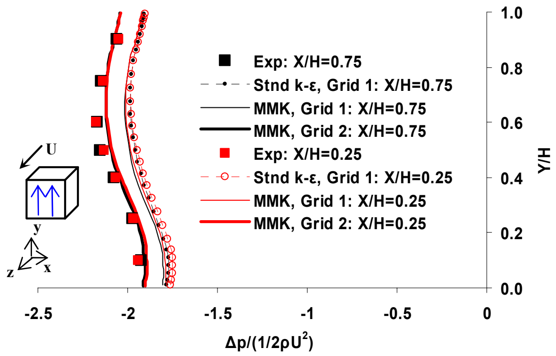

a)

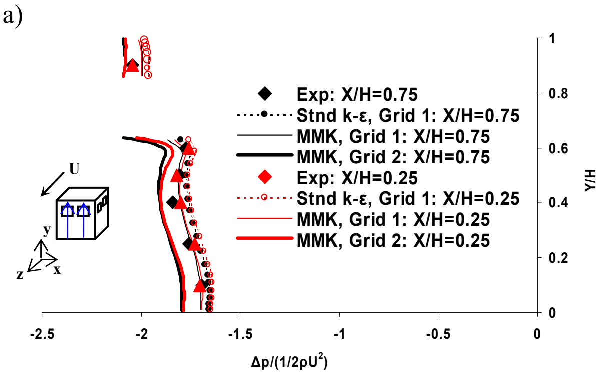

b)

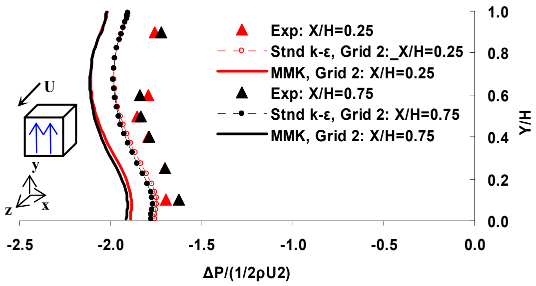

c)

Fig. 10. Figure caption on facing column

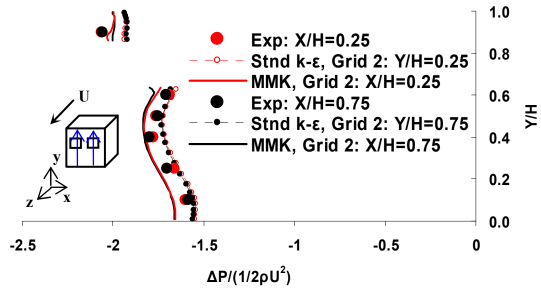

d)

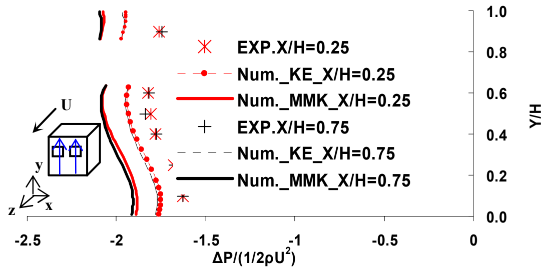

e)

Fig. 10. (continued) Pressure distribution on the downstream face at 0.25 and 0.75 of the cube width for a) solid cube, b) cube with openings on all faces (Fig. 1), c)cube with openings on the upwind face, d) cube with openings on the upwind and downstream faces, and e) cube with openings on the downstream face.

For the downstream face (Fig. 10), numerical calculations indicate that, in the absence of through-flow, the pressure distribution on the downstream face is very similar to that of the solid cube case with a strong recirculation forming behind the cube. However, there is an inconsistency in this conclusion when the experimental measurements are considered. The measured pressure distribution on the downstream face shows lower pressure levels when either the upstream or downstream openings are present (Fig. 10c,e) and not only when there is through-flow (Fig. 10b,d). Further accuracy in both the numerical and experimental approaches is required to explain this result.

Along the side face, in the absence of the through- flow (Fig. 11 a,d), a large amount of the flow is forced along the sides and leads to lower pressures than when the openings allow flow through the cube (Fig. 11 b,c). Furthermore, the presence of the openings on the side faces does not seem to significantly influence the local flow since the pressure distribution both at 0.25 and 0.75 of the cube height remains similar. The differences that do arise for the different positioning of the openings can therefore be attributed to the change in the flow pattern due to the flow, or not, through the cube.

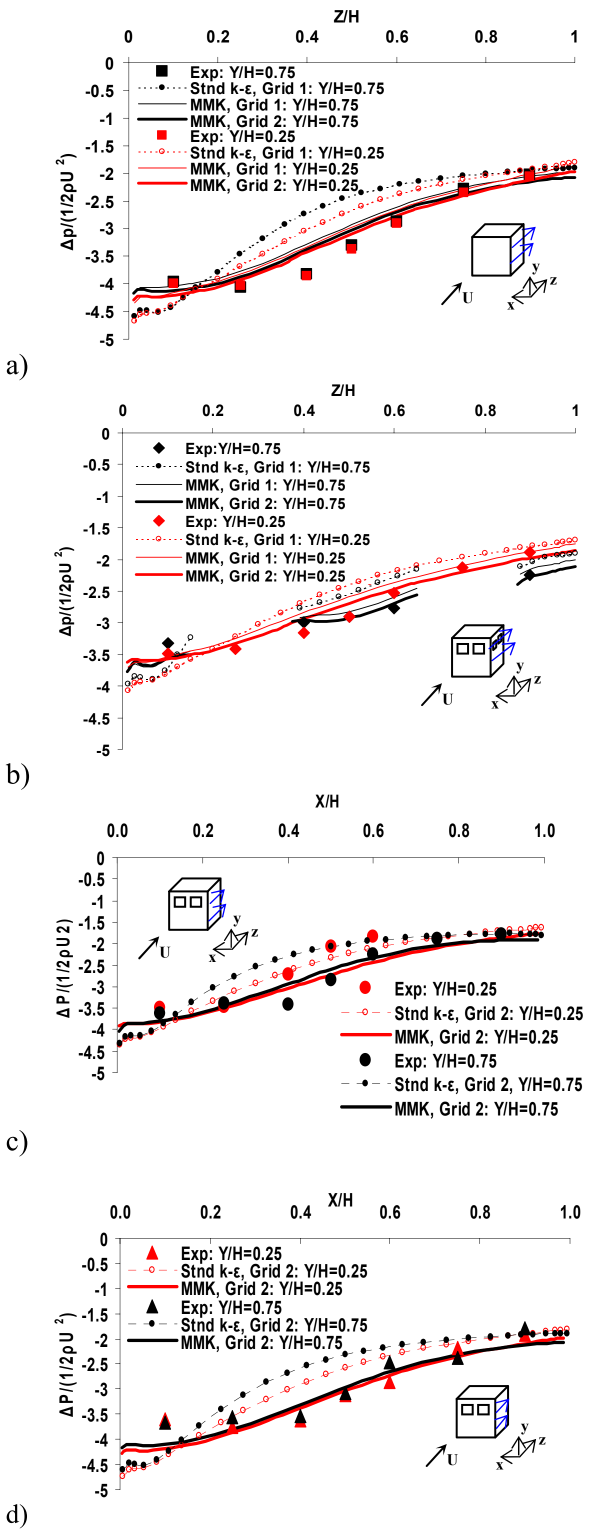

Fig. 11. Pressure distribution on the side face at 0.25 and 0.75 of the cube height for a) solid cube, b) cube with openings on all faces (Fig. 1), c)cube with openings on the upwind and downstream faces, and d)cube with openings on the upwind face.

From the comparison between the results of the numerical calculations and the experimental measurements, it can safely be concluded that the MMK modification to the k-ε model leads to a significant improvement in this type of confined flow. Generally, better agreement is evident in the numerical prediction of pressure distribution on all sides of the cube. There is a marked improvement in the prediction of the pressure distribution in the recirculation regions on the top and sides of the cube when using the MMK model, both in regard to size and pressure values (Fig. 8 andFig. 11). It should also be noted that the improvement is achieved when using the same level of spatial discretisation (grid size), and that increasing the grid density leads to slightly better accuracy. In Fig. 11, the results obtained by implementation of the MMK model using the coarser grid show minimal improvement at increased grid density. The top and side faces are those most influenced by the flow separating from the horizontal and vertical leading edges after having stagnated at the upstream face. The generated turbulence kinetic energy near the upstream edges will greatly influence the separation phenomenon and it seems that the MMK model shows better behaviour in modeling this.

The numerical prediction of pressure distributions all along the upstream and downstream faces is not significantly altered by the modification to the turbulence model. Here, most of the improvement in accuracy is seen to arise from the increase in spatial discretisation density (Fig. 9- Fig. 11). Generally, as explained previously, improvement is gained in regions closer to the separation that follows the front stagnation region at the leading edges and this is in accordance with the initial implementation of this modification ([3]).

Openings	V'/V'_{up}
All four faces	0.0950
Upstream and downstream faces	0.0685
Upstream face	0.0016
Downstream face	≅0

Table 1. Non dimensional Volume flux that enters the cube through the openings

Based on the results of the numerical calculations, the volume flux entering (and therefore exiting) the cube from all openings has been calculated by integrating across all openings. The calculated volume flux is non-dimensionalised by the upstream flux ($V'=U\cdot H^2$) and presented in Table 1. From these results it can be concluded that, as expected, openings allowing cross flow will lead to higher flow rates through the cube and that in this case, the presence of side openings leads to an increase of 38%. If no cross flow is allowed then the upstream openings will lead to higher air flow through the cube.

5 Conclusions

Experimental measurements and numerical predictions have been performed regarding the flow past a solid cube and a cube with a combination of openings on all four sides under highly confined conditions. The main objective was to provide reliable data for validation of numerical modeling methodologies targeted at the study of infiltration and natural ventilation of buildings. The configuration can also be thought of as resembling that of the close proximity of neighbouring structures.

Under the level of confinement that the studies were performed, the openings mainly influence the pressure distribution at the top and upper levels of the cube while leaving the lower levels relatively undisturbed. Since the openings allow for flow through the building, the strong upstream stagnation and flow acceleration along the top and sides are slightly damped. The presence of openings on the sides enhances through-flow by almost 40%, when opposing openings are present. On the other hand, for single sided openings i.e. upstream or downstream, surface pressure distributions resemble those of the solid cube and lead to minimal air exchange between the inside and outside of the cube. However, this observation may be significantly different if thermal forces due to buoyancy are included in the analysis.

On the part of the numerical methodology, the MMK modification to the standard k-ε turbulence model, which aims to correct the k-ε model weakness in predicting turbulence kinetic energy production in flow stagnation regions, leads to a significant improvement in the level of agreement with the measurements. This is most pronounced in regions that are highly dependent on flow separation following stagnation. Other regions, i.e. upstream stagnation and downstream recirculation, have most to gain from increased spatial discretisation.

Acknowledgements

The authors would like to acknowledge funding of the present research by the EU and the Greek Ministry of Education and Religious Affairs. The contribution of Mr. Pantelis Koutselakis is also appreciated.

References:

[1] Tuomaala P. and Rahola J. Combined air flow and thermal simulation of buildings. Building and Environment, Vol. 30, No. 2, 1995, pp. 225-265.

[2] Chena H., Ookaa R., Harayamaa K, Kato S, Li X, Study on outdoor thermal environment of apartment block in Shenzhen, China with coupled simulation of convection, radiation and conduction. Energy and Buildings, Vol. 36, No. 12, 2004, pp. 1247-1258

[3] Tsuchiya M., Murakami S., Mochida A., Kondo K. and Ishida Y. Development of A New k-ε Model For Flow And Pressure Fields Around Bluff Body. J. of Wind Engineering and Industrial Aerodynamics. Vol. 67&68, 1997, pp. 169-182.

[4] Jiang Y., Alexander D., Jenkins H., Arthur R., Chen Q. Natural ventilation in buildings: measurement in a wind tunnel and numerical simulation with large-eddy simulation. J of Wind Engineering and Industrial Aerodynamics. Vol. 91, 2003, pp. 331–353.

[5] Patankar S. and Spalding D. A Calculation Procedure for Heat, Mass and Momentum Transfer in Three Dimensional Parabolic Flows. Int. J. Heat Mass Transfer. Vol. 15, 1972, pp. 1787

[6] Rhie C. and Chow W. Numerical Study of the Turbulent Flow Past an Airfoil with Trailing Edge Seperation. AIAA J. Vol. 21, 1983, pp. 1525-1532

[7] Papadakis G. and Bergeles G. A Locally Modified Second Order Upwind Scheme for Convection Terms Discretisation. Int. J. Num. Meth. Heat Fluid Flow, Vol. 5, 1995, pp. 49-62.